Postfach 10 11 61
69451 Weinheim
Germany
Courier services:
Boschstraße 12
69469 Weinheim
Germany
Tel.: (+49) 6201 606 235
Fax: (+49) 6201 606 500
E-mail: **advmat@wiley.com**

Dear Author,

Please correct your galley proofs carefully and return them no more than four days after the page proofs have been received.

Please limit corrections to errors already in the text; cost incurred for any further changes or additions will be charged to the author, unless such changes have been agreed upon by the editor.

The editors reserve the right to publish your article without your corrections if the proofs do not arrive in time.

Note that the author is liable for damages arising from incorrect statements, including misprints.

Please note any queries that require your attention. These are indicated with a Q in the PDF and a question at the end of the document.

Reprints may be ordered by filling out the accompanying form.

Return the reprint order form by fax or by e-mail with the corrected proofs, to Wiley-VCH : **advmat@wiley.com**

To avoid commonly occurring errors, **please ensure that the following important items are correct** in your proofs (please note that once your article is published online, no further corrections can be made):

- **Names** of all authors present and spelled correctly
- **Titles** of authors correct (Prof. or Dr. only: please note, Prof. Dr. is not used in the journals)
- **Addresses** and **postcodes** correct
- **E-mail address** of corresponding author correct (current email address)
- **Funding bodies** included and grant numbers accurate
- **Title** of article OK
- All **figures** included
- **Equations** correct (symbols and sub/superscripts)

Corrections should be made directly in the PDF file using the PDF annotation tools. If you have questions about this, please contact the editorial office. The corrected PDF and any accompanying files should be uploaded to the journal's Editorial Manager site.

Author Query Form

WILEY

Journal ADMA

Article adma202000566

Dear Author,

During the copyediting of your manuscript the following queries arose.

Please refer to the query reference callout numbers in the page proofs and respond to each by marking the necessary comments using the PDF annotation tools.

Please remember illegible or unclear comments and corrections may delay publication.

Many thanks for your assistance.

Query No.	Description	Remarks
Q-OO	Open access publication of this work is possible via Wiley OnlineOpen. Information about this is available at: https://authorservices.wiley.com/author-resources/Journal-Authors/licensing-open-access/open-access/onlineopen.html. The cost of publishing your manuscript OnlineOpen may be covered by one of Wiley's national agreements. To find out more, visit https://authorservices.wiley.com/author-resources/Journal-Authors/open-access/affiliation-policies-payments/index.html. Note that eligibility for fee coverage is determined by the affiliation of the primary corresponding author designated at submission. Please log in to your Wiley Author Services account at https://authorservices.wiley.com/ and confirm your affiliation to see if you are eligible. Instructions for placing an OnlineOpen order can be found at: https://authorservices.wiley.com/author-resources/Journal-Authors/open-access/how-to-order-onlineopen.html. To publish your article open access, please complete the order process before completing your proof corrections.	
Q1	Please confirm that forenames/given names (blue) and surnames/family names (vermilion) have been identified correctly.	
Q2	Please provide the highest academic title (either Dr. or Prof.) for all authors, where applicable.	
Q3	Please define all acronyms at their first appearance in the abstract, text and table of contents, respectively. Only expanded forms are allowed if the elements are cited only once in the article.	
Q4	Please check all equations have been correctly typeset.	
Q5	The term 'et al.' is not permitted in the reference list. Please provide all author names in ref. [3].	
Q6	Please provide authors names in ref. [8], if applicable.	

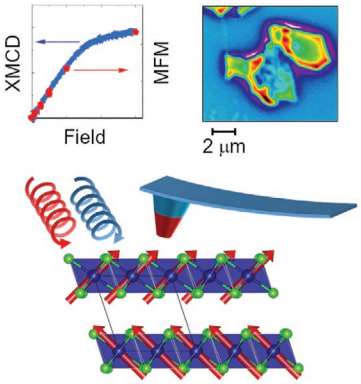

Low-temperature magnetic force microscopy (MFM) and X-ray ~~circular magnetic~~ dichroism are used to investigate micromechanically cleaved flakes of chromium trichloride crystals, highlighting a ninefold increase of antiferromagnetic coupling between layers after exfoliation. Joint topographic and magnetic measurements by MFM on individual flakes show a common behavior in the 10–50 nm thickness range.

ADVANCED MATERIALS
www.advmat.de

Enhancement of the Magnetic Coupling in Exfoliated $CrCl_3$ Crystals Observed by Low-Temperature Magnetic Force Microscopy and X-Ray Circular Dichroism

Michele Serri,* Giuseppe Cucinotta, Lorenzo Poggini, Giulia Serrano, Philippe Sainctavit, Judyta Strychalska-Nowak, Antonio Politano, Francesco Bonaccorso, Andrea Caneschi, Robert J. Cava, Roberta Sessoli, Luca Ottaviano, Tomasz Klimczuk, Vittorio Pellegrini, and Matteo Mannini*

Magnetic crystals formed by 2D layers interacting by weak van der Waals forces are currently a hot research topic. When these crystals are thinned to nanometric size, they can manifest strikingly different magnetic behavior compared to the bulk form. This can be the result of, for example, quantum electronic confinement effects or the presence of defects or pinning of the crystallographic structure in metastable phases induced by the exfoliation process. In this work, an investigation of the magnetism of micromechanically cleaved $CrCl_3$ flakes with thickness >10 nm is performed. These flakes are characterized by superconducting quantum interference device magnetometry, surface-sensitive X-ray magnetic circular dichroism, and spatially resolved magnetic force microscopy. The results highlight an enhancement of the $CrCl_3$ antiferromagnetic interlayer interaction that appears to be independent of the flake size when the thickness is tens of nanometers. The estimated exchange field is 9 kOe, representing an increase of ≈900% compared to the one of the bulk crystals. This effect can be attributed to the pinning of the high-temperature monoclinic structure, as recently suggested by polarized Raman spectroscopy investigations in thin (8–35 nm) $CrCl_3$ flakes.

Layered crystals held together by van der Waals (vdW) forces feature peculiar physical properties due to the unbalance between the strong in-plane interactions, determined by the 2D network of covalent bonds, and the weak interlayer ones. Top-down exfoliation and bottom-up growth protocols used in such materials permit to produce high aspect ratio 2D crystals with thicknesses down to single or few atomic layers.[1] A large number of vdW materials have been studied experimentally or theoretically, finding an abundance of different functional properties that can also be tuned depending on the thickness of the produced samples.[2,3] Recently, vdW materials that exhibit ferromagnetic order in ultrathin crystals[4–7] have attracted increasing attention as potential building blocks of spintronic devices in 2D heterostructures.[8–12] In these devices,

Dr. M. Serri, Dr. F. Bonaccorso, Dr. V. Pellegrini
Istituto Italiano di Tecnologia–Graphene Labs
via Morego 30, Genova 16163, Italy
E-mail: michele.serri@iit.it

Dr. G. Cucinotta, Dr. L. Poggini, Dr. G. Serrano, Prof. R. Sessoli, Prof. M. Mannini
Chemistry Department "U. Schiff" and INSTM RU
Università degli studi di Firenze
Via della Lastruccia 3-13, Sesto Fiorentino 50019, Italy
E-mail: matteo.mannini@unifi.it

Dr. G. Serrano, Prof. A. Caneschi
Department of Industrial Engineering
DIEF, and INSTM RU
Università degli Studi di Firenze
Via di S. Marta 3, Firenze 50139, Italy

Dr. P. Sainctavit
Institut de Mineralogie, de Physique des Materiaux et de Cosmochimie
UMR 7590, CNRS
Sorbonne Université, MNHN
Paris F-75005, France

Dr. P. Sainctavit
Synchrotron SOLEIL
L'Orme des Merisiers
Saint-Aubin-BP 48, Gif-sur-Yvette F-91192, France

J. Strychalska-Nowak, Prof. T. Klimczuk
Faculty of Applied Physics and Mathematics
Gdansk University of Technology
Gdansk 80-233, Poland

Dr. A. Politano, Prof. L. Ottaviano
Dipartimento di Scienze Fisiche e Chimiche (DSFC)
Università dell'Aquila
Via Vetoio 10, L'Aquila 67100, Italy

Dr. A. Politano, Prof. L. Ottaviano
CNR-SPIN UoS L'Aquila
Via Vetoio 46, L'Aquila 67100, Italy

Dr. F. Bonaccorso, Dr. V. Pellegrini
BeDimensional Spa
Genoa 16163, Italy

Prof. R. J. Cava
Department of Chemistry
Princeton University
Princeton, NJ 08544, USA

The ORCID identification number(s) for the author(s) of this article can be found under https://doi.org/10.1002/adma.202000566.

DOI: 10.1002/adma.202000566

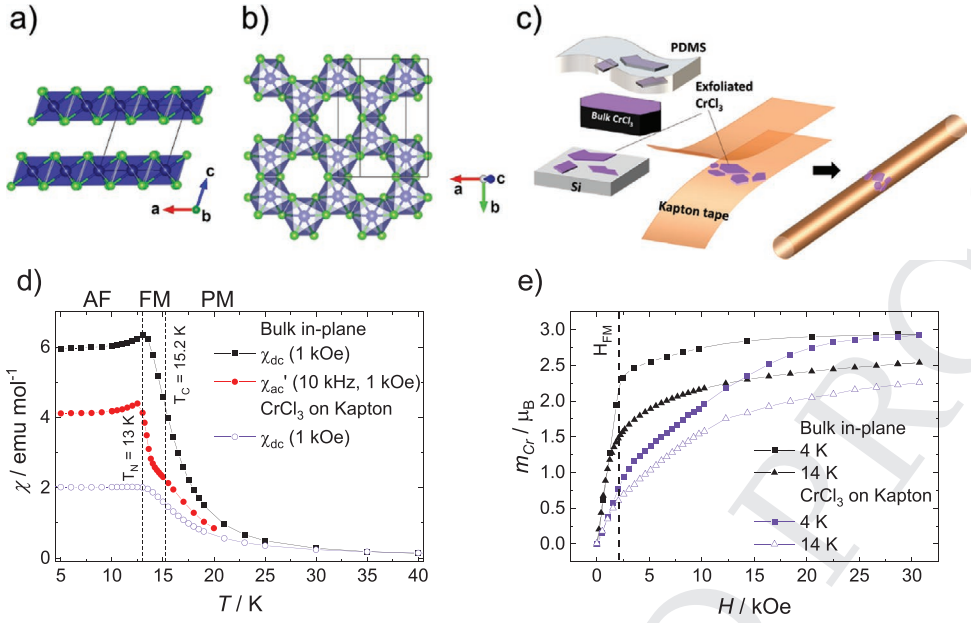

Figure 1. a) Lateral ~~projection along the *b* axis~~ of a $CrCl_3$ crystal in the monoclinic phase (green Cl, blue Cr; octahedral coordination is highlighted). b) Top view of a single $CrCl_3$ layer; axes of the monoclinic cell are indicated. c) Schematic of the crystal exfoliation and flakes transfer process on Si and Kapton substrates. d) Temperature dependence of χ in bulk (black and red dots referred to dc and ac measurements, respectively) and exfoliated $CrCl_3$ (violet empty dots) measured with magnetic field in *ab* plane; e) isothermal magnetization curves of the bulk (black) and exfoliated (violet) $CrCl_3$ measured at 4 K (squares) and 14 K (triangles) with magnetic field in *ab* plane; the dashed line highlights the field H_{FM} corresponding to the transition to a ferromagnetic-like state in bulk at 4 K.

the spin degree of freedom is controlled and manipulated in order to enable new quantum modes of operation for logic devices[11,13] and sensors [14,15] improving efficiency and speed.[16] Among magnetic materials interesting for 2D scalability,[17] chromium trihalides (CrX_3) crystals represent a class of semiconducting layered materials with potential applications in optoelectronics[12] and spintronics,[11,13–15,18,19], e.g., as circularly polarized light emitters[12] and magnetic tunnel junctions.[19–21] Individual layers of CrX_3 are composed by a Cr sheet forming a honeycomb net, sandwiched between two halide sheets, where Cr^{3+} cations in $S = 3/2$ spin state are octahedrally coordinated by six halide X^- anions, and each anion is shared between two cations (**Figure 1**a,b) resulting in an intra-layer ferromagnetic exchange interaction.[22] Two types of layer stacking arrangement, monoclinic and rhombohedral, have been observed in bulk CrX_3 crystals, depending on the X element and temperature.[23] The investigation of the effect of nanostructuring (i.e., in both lateral size and thickness) and exfoliation processes on the magnetic properties of these vdW materials is crucially important for their exploitation in spintronic devices.

Several reports[4,13–15] have shown that thin (0.7–14 nm, i.e., 1–20 layers) CrI_3 flakes exhibit antiferromagnetic interlayer coupling, in contrast with the ferromagnetic interaction in the bulk counterpart.[24] As of late, a tenfold enhancement of antiferromagnetic exchange was reported in exfoliated $CrCl_3$ few layer (1–4) flakes compared to the pristine bulk crystal.[21] Experimental evidence suggests that interlayer magnetism is insensitive to the thickness of the CrX_3 exfoliated flakes, at least when this is less than ≈14 nm.[14] Recent experimental[21] and theoretical[10,25,26] investigations have suggested that the magnetic properties of the exfoliated CrX_3 flakes derive ~~from a crystallographic difference from~~ the pristine bulk crystals.[10,21,25,26] In fact, ab initio calculations predict a stronger antiferromagnetic exchange in the monoclinic phase compared to the rhombohedral one,[10,25,26] while polarized Raman experiments (at the ≈247 cm^{-1} mode) on $CrCl_3$ flakes (8–35 nm)[21] indicate the absence of the low-temperature ($T < 235$ K) rhombohedral phase, which is contrarily observed in bulk.[27] The origin of this phenomenon is still under debate. It has been speculated that the phase transition is hindered in the exfoliated flakes by stacking faults and other defects induced by the exfoliation process.[21] An alternative explanation invokes the existence of a surface phase on CrX_3 crystals, which is found both in exfoliated and pristine crystals, but is masked in the latter by the prevailing bulk phase.[14] A deeper investigation of these materials, based on the comparison of bulk magnetometric analysis with the information achieved through surface-sensitive magnetic techniques, is mandatory for a sound assignment of the local magnetic state.

Here, we unravel the magnetic properties of micromechanically cleaved chromium trichloride ($CrCl_3$) crystals having thickness of the order of tens of nanometers. We use low-temperature magnetic force microscopy (MFM), as a local magnetic probe, flanked by angle-resolved X-ray magnetic circular dichroism (XMCD) and superconducting quantum interference device (SQUID) magnetometry. While previous studies focused on the magnetism of ultrathin flakes (<9 nm),[21,28,29] our multitechnique study presents a detailed characterization of pristine and exfoliated $CrCl_3$ in the thickness range ≈10–50 nm. Our results show that micromechanical cleavage determines, even at the mesoscopic thickness of 10–50 nm thickness—a scale of technological relevance—a significant change in the magnetic

properties of the $CrCl_3$ crystal. A clear example is the increase of the saturation field at low-temperature (4–14 K) compared to the bulk counterpart. Besides, these changes are not associated with an anomalous behavior of the surface layers.

Chromium trichloride ~~($CrCl_3$)~~ is the most stable among the ~~chromium trihalide~~ materials, offering significant advantages in processability compared to the iodide and bromide ones, which suffer from rapid (<15 min for CrI_3) attack by atmospheric air.[14] In the bulk form, $CrCl_3$ layers at room temperature are stacked according to a monoclinic phase (space group $C2/m$; Figure 1a,b), as confirmed here by the X-ray diffraction pattern (see Figure S1 in the Supporting Information) and the detected Raman modes (Figure S2, Supporting Information). Bulk $CrCl_3$ crystals exhibit at low-temperature (≈15 K) two magnetic transitions that we observed by temperature dependent dc magnetic susceptibility (χ_{dc}) measurements (Figure 1d). The maximum of the slope ($-d\chi/dT$) at 15.2 and 15.5 K, detected with the field in-plane, i.e., parallel to $CrCl_3$ layers and the crystal ab plane (Figure 1d), and out-of-plane (Figure S3a, Supporting Information) respectively, identifies the paramagnetic-2D ferromagnetic transition temperature T_C,[30] which results in ferromagnetic order within individual layers. The transition from 2D ferromagnetic to 3D antiferromagnetic, i.e., the antiparallel arrangement of the moments of neighboring layers, is picked up by the zero of $d\chi_{dc}/dT$ at T_N = 13 K (field in-plane) and 13.7 K (field out-of-plane). These magnetic transitions can also be revealed by ac susceptibility measurements[31] (Figure 1d; Figure S3a, Supporting Information). The transitions are sensitive to the internal field; therefore different values of the external field (here 1 kOe) or crystal orientations (due to demagnetizing factors) yield slightly different transition temperatures, which can justify the slight differences with literature values (T_C ≈ 17 K; T_N = 15.5 K).[27,32–34] As expected, isothermal magnetization curves of the bulk crystal (Figure 1e; Figure S3b, Supporting Information) are in agreement with previous studies.[27,32,33] At 4 K the in-plane magnetization rises linearly with field, corresponding to the progressive canting of the magnetization of the two antiferromagnetically coupled sub-lattices, until, at field strength H_{FM} ≈ 2 kOe, the magnetic sublattices become aligned with the external field in a ferromagnetic-like state. Above H_{FM}, the magnetization increases until reaching a saturation moment of 3 Bohr magnetons (μ_B) per Cr atom (μ_B) at 30 kOe, in agreement with S = 3/2 for a trivalent Cr.

To investigate flakes, a $CrCl_3$ bulk crystal was exfoliated inside a nitrogen-filled glovebox, by repeated cleaving with an adhesive ~~PDMS~~ film (Figure 1c). The exfoliated $CrCl_3$ flakes were transferred onto a Si (100) chip and onto a Kapton adhesive tape. The $CrCl_3$ flakes on Si were analyzed by atomic force and optical microscopy, determining a thickness of 35 ± 20 nm with lateral sizes of 4 ± 2 µm (see Figure S4 in the Supporting Information). The chemical stability of the exfoliated crystals deposited onto Si was confirmed by X-ray photoelectron spectroscopy (XPS) in the Cr 2p and Cl 2p regions, which shows virtually identical components in bulk and exfoliated $CrCl_3$ flakes, and in line with what reported for polycrystalline samples (see X-ray photoelectron spectroscopy section; Figure S5 and Table S1, Supporting Information).[35]

The magnetic properties of flakes on Kapton were first evaluated using SQUID magnetometry limited to the in-plane field configuration (see Figure 1d and Methods for details in the Supporting Information). The temperature dependence of χ_{dc} (Figure 1d) evidences the persistence of the magnetic transitions noticed in the pristine $CrCl_3$ material. In particular, the ferromagnetic transition (determined from $d\chi/dT$) is observed in these flakes at 16 K, while antiferromagnetic one at 13.6 K. Notably, differences ~~of~~ the exfoliated $CrCl_3$ flakes ~~compared to~~ the bulk sample can be found in the isothermal magnetization curves (Figure 1e), revealing that thinning by exfoliation affects the in-plane magnetic properties of the crystal. The magnetization in the exfoliated $CrCl_3$ flakes rises with the applied field at a slower rate compared to the bulk. The curve changes slope at 2 kOe, indicating the presence of multiple contributions. These could be explained by the presence of $CrCl_3$ flakes with different thicknesses, a part of them still exhibiting a bulk-like behavior.

To gain insights into the magnetic behavior of the $CrCl_3$ flakes, we performed low-temperature XMCD investigations (**Figure 2**a; Figure S6, Supporting Information). X-ray magnetic circular dichroism overcomes the limits of traditional magnetometry in terms of both selectivity and sensitivity because the dichroic signal for transition metal-based systems is, in a good approximation, proportional to the average magnetic moment of the absorbing element at the temperature, field ~~strength~~ and relative orientation of the sample with respect to the X-ray beam direction ~~of~~ the investigation.[36] X-ray absorption spectroscopy (XAS) spectra were recorded with opposite circularly polarized light at 4 and 14 K under an external magnetic field of 30 kOe at the Cr $L_{2,3}$ edges.[37,38] We observe a strong negative dichroic signal at 575.9 eV that, for normal incidence, corresponds to ≈120% (Figure S7, Supporting Information) and ≈128% (Figure 2a) of the edge jump for the bulk crystal and the exfoliated flakes, respectively, consistent with a magnetic moment of about 3 μ_B per Cr atom.[39,40] X-ray absorption spectroscopy and XMCD line shapes are in agreement with an octahedral Cr^{3+} found in other compounds (Figure S8, Supporting Information).[41,42]

The value of the maximum of the XMCD signal was then monitored during a sweep of the magnetic field between 30 and −30 kOe to obtain the magnetization curve ($I_{XMCD}(H)$) of the $CrCl_3$ flakes (Figure 2b,c). These measurements were performed at normal (0°) and grazing (60°) incidence, with respect to the sample surface, to highlight the differences between the out-of-plane and in-plane behavior of the flakes. These differences were not accessible through SQUID measurements due to experimental constraints. At grazing incidence (whose configuration mostly resembles the SQUID in-plane measurements) the $I_{XMCD}(H)$ (Figure 2b) is qualitatively similar to the $M(H)$ measured on the $CrCl_3$ flakes on Kapton at 4 and 14 K (Figure 1e). In particular, one can recognize a similar change of the slope around 2 kOe, followed by an almost linear increase in the magnetization, which approaches saturation just below 20 kOe. The $I_{XMCD}(H)$ curve obtained at normal incidence (Figure 2c) shows an analogous behavior, which overlaps almost perfectly with the measurement at grazing incidence after accounting for the anisotropy due to the flakes aspect ratio (Figure S9, Supporting Information; see Demagnetizing Field Correction Methods in the Supporting Information). The agreement between the SQUID and variable magnetic field XMCD

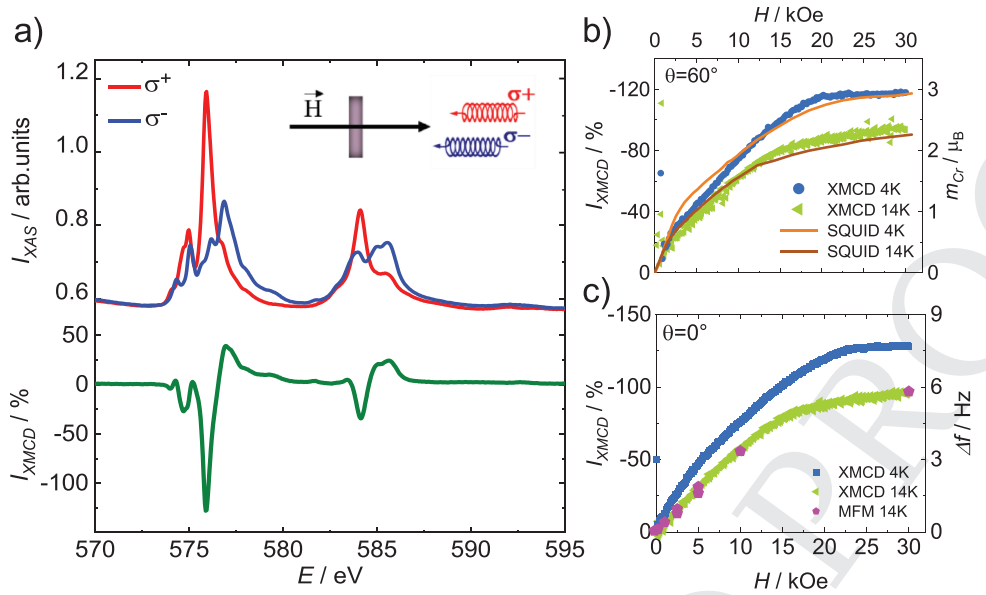

Figure 2. a) XAS and XMCD spectra obtained on the exfoliated sample on Si at the Cr $L_{2,3}$ edge with $H = 30$ kOe, $T = 4$ K and normal incidence ($\theta = 0°$), red line and blue line are σ^+ and σ^-, respectively, green line is XMCD; b) isothermal (4 K blue and 14 K green) XMCD measurements at grazing incidence ($\theta = 60°$) of the $CrCl_3$ flakes on Si, compared with SQUID magnetometry (4 K orange and 14 K brown) of the flakes on Kapton; c) isothermal (4 K blue and 14 K green) XMCD measurements at normal incidence of the $CrCl_3$ flakes on Si, compared with field dependence of the MFM contrast (magenta points).

characterizations on the exfoliated samples is striking. It confirms that the micromechanical cleavage of the crystal to obtain $CrCl_3$ flakes with nanometric thickness induces a modification of the low-temperature magnetic properties of the material rather than increasing surface effects.

Magnetic force microscopy maps gradients of the stray field of the magnetized sample.[43] The MFM signal at each point is proportional to the local magnetization of the flake times a geometric factor that depends on the magnetization of the tip and its relative position with respect to the flake. Previous works by our group and others have shown that this technique can be used to obtain magnetization curves of magnetic microstructures of molecular magnets, provided that either the tip magnetization does not change during the field scan or its change is well characterized.[44,45]

Here, in order to characterize the magnetic behavior of individual flakes and locally discriminate the contribution of flake thickness, we performed in parallel AFM and MFM measurements (**Figure 3**). We adopted the same preparation procedure of the flakes on silicon described above and we performed MFM characterization at 14 K, close to the χ maximum. Figure 3a shows the AFM image of the sample. The feature at the center of the area may consist of two overlapping $CrCl_3$ flakes or a single folded flake of ≈25 nm thickness. A perpendicular (out-of-plane) magnetic field of 50 kOe at 14 K was applied and a map of the magnetic force was acquired at a probe lift height of 100 nm. A clear magnetic contrast is observed in Figure 3b, highlighting regions of attractive magnetic interaction inside the flakes and repulsive force just outside the border of the flakes. The findings are consistent with the fact that the $CrCl_3$ flakes are perpendicularly magnetized by the field, which creates a re-entrant stray field outside of the flake. As expected, the MFM signal reaches its maximum in regions where the magnetization or the thickness is discontinuous, such as the flake borders, while it is minimum inside the flakes, akin to a uniformly magnetized infinite plane, which does not generate any stray field.[46] Magnetic force microscopy measurements repeated at decreasing field strengths have shown progressive fading of the magnetic features (Figure 3c). A very weak contrast is still observable after a demagnetization cycle, which must be attributed to spurious electrostatic or van der Waals forces, despite compensation of the contact potential (for more details see Magnetic Force Microscopy Methods ~~in the~~ in the Supporting Information). To quantitatively monitor the magnetic contrast as a function of the field we have followed a similar protocol adopted for a patterned deposit of single molecule magnets.[44] We estimated the MFM contrast from spatial profiles of the frequency shift maps along three paths, indicated by the dotted lines in the topography and MFM images (see Figure 3a,b). As noticed from the topographic contrast, the selected paths intersect regions of different height (Figure 3d, bottom), thus justifying the complex dependence on the spatial coordinate of the corresponding MFM profiles shown at the top of Figure 3d. However, one can extract from this data a contrast Δf defined here as the difference between the maximum and the minimum of the MFM signal detected around the lower edge of the flake. By studying the field dependence of Δf we observe similar trends in all of the three profiles considered, as highlighted in Figure 3e by the overlap of the MFM contrast curves after normalization. This behavior is in line with the one observed with the average measurements on the exfoliated material; for instance the $\Delta f(H)$ curve extracted from one of these sets (path 1, thickness = 32 ± 3 nm) almost perfectly overlaps with the 14 K XMCD data at normal incidence (Figure 2c). Our results suggest that the saturation field of the $CrCl_3$ flakes is independent of the number of layers in the range of thickness considered here. We ~~also~~ found that the saturation value of Δf,

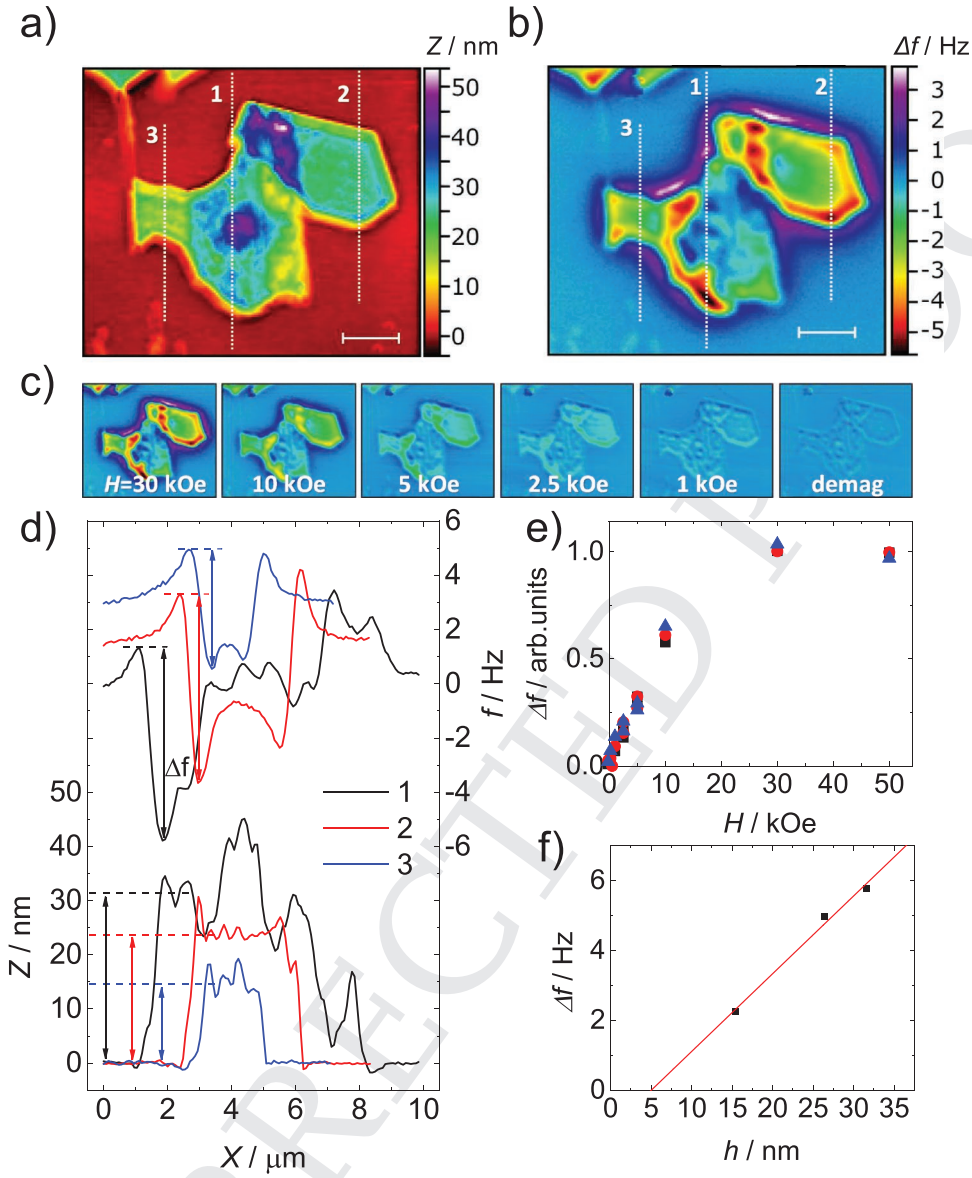

Figure 3. a) AFM image of exfoliated $CrCl_3$ flakes on Si; b) MFM image of the region in a), measured at 50 kOe and 14 K; the numbered dotted lines in (a) and (b) indicate the profiles along which the MFM signal was analyzed; c) MFM images acquired at 14 K and magnetic fields between 30 kOe and 0 Oe (demagnetized state); d) MFM contrast (top) and AFM topography (bottom) along the profiles indicated in (a) and (b); e) normalized MFM contrast in the three profiles as a function of applied field at 14 K; f) correlation between the thickness of the flakes along the three profiles and the respective saturation MFM signal measured at 50 kOe and 14 K.

that is proportional to the aerial density of magnetic moment of the flake at saturation, follows~~, as expected,~~ an apparent linear dependence with respect to the flake thickness (see Figure 3f). An offset of ≈5 nm to the "true" thickness value can be explained by the additional height introduced by the interface between ~~the~~ flake and ~~the~~ substrate.[47]

Our study highlights MFM as a key technique for the investigation of 2D materials. While SQUID magnetometry probed the whole ensemble of exfoliated flakes, MFM provided magnetic and topographic information with nanometric resolution that were used to correlate the behavior of flakes with their thickness. Compared to magneto-optical methods, MFM has higher spatial resolution and offers a simultaneous measurement of the flake area and thickness, facilitating systematic investigations of size-dependent effects in 2D magnets.

The ~~results of the~~ MFM characterization support our interpretation of the XMCD and SQUID results, and the hypothesis that the exfoliated $CrCl_3$ flakes with a thickness of tens of nanometers exhibit magnetic saturation at higher fields compared to the bulk counterpart. This difference could be due to magnetic interactions contrasting the alignment of the spins with the magnetic field, such as an increase of the antiferromagnetic exchange term or of the magnetocrystalline anisotropy compared to the unexfoliated $CrCl_3$ crystal. We tend to rule out the latter effect because the identical shape of the Cr multiplet in XAS experiments suggest very similar Cr coordination in

the exfoliated and pristine crystal. Moreover, angle-dependent XMCD measurements show only minor differences between the normal and grazing incidence measurements that can be explained by shape anisotropy (i.e., demagnetizing field) in the high aspect ratio flakes (lateral size/thickness ratio of ≈100).

The main effect observed after the exfoliation process on the $CrCl_3$ flakes, i.e., the increase of the saturation field, is thus caused by an enhancement of the antiferromagnetic coupling compared to the unexfoliated crystal. Following the classical treatment of Klein et al.[21] and Wang et al.,[48] the strength of the interlayer interaction can be quantified by an effective exchange field H_e, which, together with the Zeeman and magnetic anisotropy interactions, contributes to the micromagnetic energy U per unit volume as in the following expression (in the cgs system)

$$U(H) = M_s \frac{H_e}{2} \sum_{i=1}^{N-1} \hat{m}_i \cdot \hat{m}_{i+1} - M_s \sum_{i=1}^{N} \vec{H} \cdot \hat{m}_i + K M_s^2 \sum_{i}^{N} \hat{m}_i \cdot \hat{z} \quad (1)$$

where H is the in-plane applied field, M_s is the (volume) saturation magnetization, N is the number of layers in the flake, $\hat{m}_i$ is a unitary vector representing the magnetization orientation in the ith layer, $\hat{z}$ is the unitary vector in the out-of-plane direction, and K is the magnetocrystalline anisotropy constant, which is considered negligible in $CrCl_3$.[27,48] The field H_{FM} at which the antiferromagnetic–ferromagnetic transition occurs in the in-plane orientation is linked to the exchange field H_e and the number N of layers in the flake by the following expression[48]

$$H_{FM}(N) = 2H_e \cos^2\left(\frac{\pi}{2N}\right) \quad (2)$$

When the perpendicular orientation is considered, an additional $4\pi M_s$ term (in cgs units) is added to the right side of Equation (2), which accounts for the demagnetization field in the flake. From Equation (2) it follows that the value of H_{FM} rapidly becomes insensitive to the number of layers, converging to the thick crystal value ($H_{FM} = 2H_e$ for $N = \infty$). In fact, when $N = 5$, as in a flake that is only 3.5 nm thick, H_{FM} already reaches 90.5% of $2H_e$, while in the thickness range considered in this study (≈15–30 nm for MFM, 10–50 nm for XMCD), the model predicts H_{FM} to be >99% of the thick limit value. Therefore, we can safely neglect the dependence on N in our case and attribute any change in H_{FM} to variations in H_e. The field H_{FM} can be determined using our XMCD data from the inflection point in the $M(H)$ or $I_{XMCD}(H)$ curves at 4 K, after correcting for the demagnetizing field $4\pi M_s$ in out-of-plane direction (see experimental section). We estimate $H_e \approx 1$ kOe ($H_{FM} \approx 2$ kOe) in bulk and ≈9 kOe ($H_{FM} \approx 18$ kOe) in exfoliated $CrCl_3$ crystal, resulting in a ninefold increase in the value of H_e.

The agreement between the three techniques used in this work thus confirms that the increase of H_e is weakly dependent on the flake thickness as long as this is less than a few tens of nanometers. We can exclude that the observed increase is a surface effect, as the same field dependence was observed with a massive (SQUID) and a surface selective (XMCD) characterization technique. We remark that XAS analysis (Figure S8, Supporting Information) confirmed negligible degradation of the exfoliated sample measured at the synchrotron. It is also unlikely that the observed properties derive from quantum confinement effects, since above a thickness of ten layers, corresponding to >5.8 nm in $CrCl_3$, 2D crystals are expected to show bulk-like electronic properties.[49,50]

Our observations are in agreement with the previous hypothesis that exfoliated $CrCl_3$ rearranges in a different lattice structure compared to the bulk material at low temperature, varying the inter-layer exchange interactions.[10,21,25] This structural flexibility is probably due to the weak van der Waals interactions between the $CrCl_3$ layers, which determine a delicate energy balance governing the layer stacking. The nano-structuration of the $CrCl_3$ crystals may cause a pinning of the high-temperature monoclinic structure at low temperature, as recently proposed,[21] or possibly lead to novel metastable phases with the observed enhanced antiferromagnetic exchange. Nevertheless, we cannot exclude that other factors linked with the exfoliation process may affect the magnetic properties of the $CrCl_3$ flakes. Recent ab initio calculations have shown that a few percent of Cr vacancies in $CrCl_3$ enhances the intra-layer ferromagnetic order and cause an insulator to half-metal electronic transition.[51] It is also likely that the strain is different in the bulk and exfoliated material. Ab initio calculations on monolayers of the CrX_3 series found that a compressive strain of few percent can switch the in-plane coupling from ferromagnetic to antiferromagnetic and increase the absolute value of the exchange interaction and the magnetocrystalline anisotropy by a factor of 2–3.[52]

In conclusion, the magnetic properties of $CrCl_3$ flakes with a thickness of tens of nanometers (≈10–50 nm) and lateral sizes of several microns (≈2–6 µm) produced by micromechanical cleavage of bulk crystals were studied with multiple spectroscopic and magnetometric techniques. The exfoliated $CrCl_3$ sample has shown a reduction of the magnetic susceptibility and an increase of the ferromagnetic transition field H_{FM} at low temperature, compared to the bulk crystal. The effect was independently observed both on ensembles of $CrCl_3$ flakes by conventional superconducting quantum interference device (SQUID) magnetometry and synchrotron-based X-ray magnetic circular dichroism (XMCD) experiments, and on individual flakes by low-temperature magnetic force microscopy (MFM). These observations are in agreement with recent studies conducted with magnetotransport in tunneling junctions[21,28,29,48] and magneto-optical measurements,[28] which highlighted that ultrathin flakes of chromium trihalides exhibit different magnetic interactions compared to the pristine bulk crystals.

Based on the experimental evidences, we can infer that the antiferromagnetic exchange interaction in the exfoliated phase is stronger than in the bulk crystal, suggesting several possible mechanisms for the explanation of this effect. It is worth noticing that low-temperature MFM was applied here—for the first time—to spatially resolve field-dependent magnetization of van der Waals crystals with thickness of few tens of nanometers.

The joint experimental investigation by conventional magnetometry, XMCD and MFM provided compatible magnetization dependences, validating the use of MFM for the characterization of exfoliated van der Waals magnetic crystals. This study opens the way to the investigation of magnetic ordering and transitions in 2D crystals and heterostructures of even lower thickness with nanometric spatial resolution.

Supporting Information

Supporting Information is available from the Wiley Online Library or from the author.

Acknowledgements

The crystal growth at Princeton was supported by the ARO-sponsored MURI on Topological Insulators (Grant No. W911NF1210461). The authors acknowledge Fondazione Ente Cassa Risparmio di Firenze (progetto SPIN-E no. 2017.0730) and MIUR-Italy ("Progetto Dipartimenti di Eccellenza 2018–2022, ref B96C1700020008" allocated to Department of Chemistry "Ugo Schiff") for the economic support, SOLEIL for provision of synchrotron radiation facilities, and all the DEIMOS staff for assistance in using the beamline. The authors also thank the Clean Room Facility and the Materials Characterization Facility of the Italian Institute of Technology for support with sample preparation and material characterization.

Conflict of Interest

The authors declare no conflict of interest.

Keywords

honeycomb lattice, magnetism, MFM, spintronics, van der Waals

Received: January 24, 2020
Revised: March 21, 2020
Published online:

[1] F. Bonaccorso, A. Lombardo, T. Hasan, Z. Sun, L. Colombo, A. C. Ferrari, *Mater. Today* **2012**, *15*, 564.
[2] K. S. Novoselov, A. Mishchenko, A. Carvalho, A. H. Castro Neto, *Science* **2016**, *353*, aac9439.
[3] A. C. Ferrari, F. Bonaccorso, V. Falko, K. S. Novoselov, S. Roche, P. Bøggild, S. Borini, F. Koppens, V. Palermo, N. Pugno, J. A. Garrido, R. Sordan, A. Bianco, L. Ballerini, M. Prato, E. Lidorikis, J. Kivioja, C. Marinelli, T. Ryhänen, A. Morpurgo, J. N. Coleman, V. Nicolosi, L. Colombo, A. Fert, M. Garcia-Hernandez, A. Bachtold, G. F. Schneider, F. Guinea, C. Dekker, M. Barbone, Z. Sun, C. Galiotis, A. N. Grigorenko, G. Konstantatos, A. Kis, M. Katsnelson, L. Vandersypen, A. Loiseau, V. Morandi, D. Neumaier, E. Treossi, V. Pellegrini, M. Polini, A. Tredicucci, G. M. Williams, B. H. Hong, J. H. Ahn, J. M. Kim, H. Zirath, B. J. van Wees, H. van der Zant, L. Occhipinti, A. Di Matteo, I. A. Kinloch, T. Seyller, E. Quesnel, X. Feng, K. Teo, N. Rupesinghe, P. Hakonen, S. R. Neil, Q. Tannock, T. Löfwander, J. Kinaret, *Nanoscale* **2014**, *7*, 4598.
[4] B. Huang, G. Clark, E. Navarro-Moratalla, D. R. Klein, R. Cheng, K. L. Seyler, D. Zhong, E. Schmidgall, M. A. McGuire, D. H. Cobden, W. Yao, D. Xiao, P. Jarillo-Herrero, X. Xu, *Nature* **2017**, *546*, 270.
[5] Z. Fei, B. Huang, P. Malinowski, W. Wang, T. Song, J. Sanchez, W. Yao, D. Xiao, X. Zhu, A. F. May, W. Wu, D. H. Cobden, J. H. Chu, X. Xu, *Nat. Mater.* **2018**, *17*, 778.
[6] C. Gong, L. Li, Z. Li, H. Ji, A. Stern, Y. Xia, T. Cao, W. Bao, C. Wang, Y. Wang, Z. Q. Qiu, R. J. Cava, S. G. Louie, J. Xia, X. Zhang, *Nature* **2017**, *546*, 265.
[7] M. Bonilla, S. Kolekar, Y. Ma, H. C. Diaz, V. Kalappattil, R. Das, T. Eggers, H. R. Gutierrez, M.-H. Phan, M. Batzill, *Nat. Nanotechnol.* **2018**, *13*, 289.
[8] *Nat. Nanotechnol.* **2018**, *13*, 269.
[9] N. Samarth, *Nature* **2017**, *546*, 216.
[10] S. W. Jang, M. Y. Jeong, H. Yoon, S. Ryee, M. J. Han, *Phys. Rev. Mater.* **2019**, *3*, 031001.
[11] S. Jiang, L. Li, Z. Wang, K. F. Mak, J. Shan, *Nat. Nanotechnol.* **2018**, *13*, 549.
[12] K. L. Seyler, D. Zhong, D. R. Klein, S. Gao, X. Zhang, B. Huang, E. Navarro-Moratalla, L. Yang, D. H. Cobden, M. A. McGuire, W. Yao, D. Xiao, P. Jarillo-Herrero, X. Xu, *Nat. Phys.* **2018**, *14*, 277.
[13] D. R. Klein, D. MacNeill, J. L. Lado, D. Soriano, E. Navarro-Moratalla, K. Watanabe, T. Taniguchi, S. Manni, P. Canfield, J. Fernández-Rossier, P. Jarillo-Herrero, *Science* **2018**, *360*, 1218.
[14] Z. Wang, I. Gutiérrez-Lezama, N. Ubrig, M. Kroner, M. Gibertini, T. Taniguchi, K. Watanabe, A. Imamoğlu, E. Giannini, A. F. Morpurgo, *Nat. Commun.* **2018**, *9*, 2516.
[15] T. Song, X. Cai, M. W.-Y. Tu, X. Zhang, B. Huang, N. P. Wilson, K. L. Seyler, L. Zhu, T. Taniguchi, K. Watanabe, M. A. McGuire, D. H. Cobden, D. Xiao, W. Yao, X. Xu, *Science* **2018**, *360*, 1214.
[16] I. Zutic, J. Fabian, S. Das Sarma, *Rev. Mod. Phys.* **2004**, *76*, 323.
[17] M. Grönke, B. Buschbeck, P. Schmidt, M. Valldor, S. Oswald, Q. Hao, A. Lubk, D. Wolf, U. Steiner, B. Büchner, S. Hampel, *Adv. Mater. Interfaces* **2019**, *6*, 1901410.
[18] Y. Zhang, Y. Wang, P. Liao, K. Wang, Z. Huang, J. Liu, Q. Chen, J. Jiang, K. Wu, *ACS Nano* **2018**, *12*, 2991.
[19] S. Jiang, J. Shan, K. F. Mak, *Nat. Mater.* **2018**, *17*, 406.
[20] H. H. Kim, B. Yang, T. Patel, F. Sfigakis, C. Li, S. Tian, H. Lei, A. W. Tsen, *Nano Lett.* **2018**, *18*, 4885.
[21] D. R. Klein, D. MacNeill, Q. Song, D. T. Larson, S. Fang, M. Xu, R. A. Ribeiro, P. C. Canfield, E. Kaxiras, R. Comin, P. Jarillo-Herrero, *Nat. Phys.* **2019**, *15*, 1255.
[22] H. Wang, V. Eyert, U. Schwingenschlögl, *J. Phys.: Condens. Matter* **2011**, *23*, 116003.
[23] M. McGuire, *Crystals* **2017**, *7*, 121.
[24] M. A. McGuire, H. Dixit, V. R. Cooper, B. C. Sales, *Chem. Mater.* **2015**, *27*, 612.
[25] N. Sivadas, S. Okamoto, X. Xu, C. J. Fennie, D. Xiao, *Nano Lett.* **2018**, *18*, 7658.
[26] D. Soriano, C. Cardoso, J. Fernández-Rossier, *Solid State Commun.* **2019**, *299*, 113662.
[27] M. A. McGuire, G. Clark, S. KC, W. M. Chance, G. E. Jellison, V. R. Cooper, X. Xu, B. C. Sales, *Phys. Rev. Mater.* **2017**, *1*, 014001.
[28] H. H. Kim, B. Yang, S. Li, S. Jiang, C. Jin, Z. Tao, G. Nichols, F. Sfigakis, S. Zhong, C. Li, S. Tian, D. G. Cory, G.-X. Miao, J. Shan, K. F. Mak, H. Lei, K. Sun, L. Zhao, A. W. Tsen, *Proc. Natl. Acad. Sci. USA* **2019**, *116*, 11131.
[29] X. Cai, T. Song, N. P. Wilson, G. Clark, M. He, X. Zhang, T. Taniguchi, K. Watanabe, W. Yao, D. Xiao, M. A. McGuire, D. H. Cobden, X. Xu, *Nano Lett.* **2019**, *19*, 3993.
[30] S. Blundell, *Magnetism in Condensed Matter*, Oxford University Press, Oxford **2001**, pp. 85–110.
[31] M. Bałanda, *Acta Phys. Pol. A* **2013**, *124*, 964.
[32] A. Narath, H. L. Davis, *Phys. Rev.* **1965**, *137*, A163.
[33] H. Bizette, A. Adam, C. Terrier, *C. R. Acad. Sci.* **1961**, *252*, 1571.
[34] B. Kuhlow, *Phys. Status Solidi A* **1982**, *72*, 161.
[35] M. C. Biesinger, C. Brown, J. R. Mycroft, R. D. Davidson, N. S. McIntyre, *Surf. Interface Anal.* **2004**, *36*, 1550.
[36] G. Schütz, W. Wagner, W. Wilhelm, P. Kienle, R. Zeller, R. Frahm, G. Materlik, *Phys. Rev. Lett.* **1987**, *58*, 737.
[37] J.-P. Kappler, E. Otero, W. Li, L. Joly, G. Schmerber, B. Muller, F. Scheurer, F. Leduc, B. Gobaut, L. Poggini, G. Serrano, F. Choueikani, E. Lhotel, A. Cornia, R. Sessoli, M. Mannini, M.-A. Arrio, P. Sainctavit, P. Ohresser, *J. Synchrotron Radiat.* **2018**, *25*, 1727.

[38] P. Ohresser, E. Otero, F. Choueikani, K. Chen, S. Stanescu, F. Deschamps, T. Moreno, F. Polack, B. Lagarde, J.-P. Daguerre, F. Marteau, F. Scheurer, L. Joly, J.-P. Kappler, B. Muller, O. Bunau, P. Sainctavit, *Rev. Sci. Instrum.* **2014**, *85*, 013106.
[39] É. Gaudry, P. Sainctavit, F. Juillot, F. Bondioli, P. Ohresser, I. Letard, *Phys. Chem. Miner.* **2006**, *32*, 710.
[40] M. Mannini, E. Tancini, L. Sorace, P. Sainctavit, M.-A. Arrio, Y. Qian, E. Otero, D. Chiappe, L. Margheriti, J. C. Cezar, R. Sessoli, A. Cornia, *Inorg. Chem.* **2011**, *50*, 2911.
[41] G. Vinai, A. Khare, D. S. Rana, E. Di Gennaro, B. Gobaut, R. Moroni, A. Y. Petrov, U. Scotti di Uccio, G. Rossi, F. Miletto Granozio, G. Panaccione, P. Torelli, *APL Mater.* **2015**, *3*, 116107.
[42] V. Corradini, A. Ghirri, U. del Pennino, R. Biagi, V. A. Milway, G. Timco, F. Tuna, R. E. P. Winpenny, M. Affronte, *Dalton Trans.* **2010**, *39*, 4928.
[43] U. Hartmann, *Annu. Rev. Mater. Sci.* **1999**, *29*, 53.
[44] M. Serri, M. Mannini, L. Poggini, E. Vélez-Fort, B. Cortigiani, P. Sainctavit, D. Rovai, A. Caneschi, R. Sessoli, *Nano Lett.* **2017**, *17*, 1899.
[45] G. Lorusso, M. Jenkins, P. González-Monje, A. Arauzo, J. Sesé, D. Ruiz-Molina, O. Roubeau, M. Evangelisti, *Adv. Mater.* **2013**, *25*, 2984.
[46] P. J. A. van Schendel, H. J. Hug, B. Stiefel, S. Martin, H.-J. Güntherodt, *J. Appl. Phys.* **2000**, *88*, 435.
[47] S. Palleschi, G. D'Olimpio, P. Benassi, M. Nardone, R. Alfonsetti, G. Moccia, M. Renzelli, O. A. Cacioppo, A. Hichri, S. Jaziri, A. Politano, L. Ottaviano, *2D Mater.* **2019**, *7*, 025001.
[48] Z. Wang, M. Gibertini, D. Dumcenco, T. Taniguchi, K. Watanabe, E. Giannini, A. F. Morpurgo, *Nat. Nanotechnol.* **2019**, *14*, 1116.
[49] M. M. Otrokov, I. P. Rusinov, M. Blanco-Rey, M. Hoffmann, A. Y. Vyazovskaya, S. V. Eremeev, A. Ernst, P. M. Echenique, A. Arnau, E. V. Chulkov, *Phys. Rev. Lett.* **2019**, *122*, 107202.
[50] A. C. Ferrari, J. C. Meyer, V. Scardaci, C. sCasiraghi, M. Lazzeri, F. Mauri, S. Piscanec, D. Jiang, K. S. Novoselov, S. Roth, A. K. Geim, *Phys. Rev. Lett.* **2006**, *97*, 187401.
[51] Y. Gao, J. Wang, Y. Li, M. Xia, Z. Li, F. Gao, *Phys. Status Solidi RRL* **2018**, *12*, 1800105.
[52] L. Webster, J.-A. Yan, *Phys. Rev. B* **2018**, *98*, 144411.

ADVANCED MATERIALS

Reprint Order Form 2019
- please return with your proofs -

Editorial Office:

Wiley-VCH Verlag, Boschstrasse 12
69469 Weinheim, Germany

Tel.: (+49) 6201 606 235
Fax: (+49) 6201 606 500

E-mail: advmat@wiley-vch.de
http://www.advmat.de

Manuscript No. _____

Please send me and bill me for

☐ no. of **reprints** via ☐ airmail (+ 25 Euro) ☐ surface mail

☐ no. of **copies of this issue** (1 copy: 28 Euro) via ☐ airmail (+ 25 Euro) ☐ surface mail

☐ **high-resolution PDF file** (330 Euro).
My e-mail address:

_____

Please note: It is not permitted to present the PDF file on the internet or on company homepages

★**Special Offer**★ If you order 200 or more reprints you will get a PDF file for half price.

Information regarding VAT
Please note that from German sales tax point of view, the charge for **Reprints, Issues or Posters** is considered as **"supply of goods"** and therefore, in general, such delivery is a subject to German sales tax. However, this regulation has no impact on customers located outside of the European Union. Deliveries to customers outside the Community are automatically tax-exempt. Deliveries within the Community to institutional customers outside of Germany are exempted from the German tax (VAT) only if the customer provides the supplier with his/her VAT number. The VAT number (value added tax identification number) is a tax registration number used in the countries of the European Union to identify corporate entities doing business there. It starts with a country code (e.g. FR for France, GB for Great Britain) and follows by numbers.

Mail reprints /cover posters / copies of the issue to:

_____
_____
_____
_____
_____

Invoice address:

_____
_____
_____
_____
_____

Date, Signature **Stamp**

VAT no.: _____
(institutes / companies in EU countries only)

Purchase Order No.: _____

Credit Card Payment

VISA, MasterCard, AMERICAN EXPRESS
Please use the Credit Card Token Generator located at the website below to create a token for secure payment. The token will be used instead of your credit card number.

Credit Card Token Generator:
https://www.wiley-vch.de/editorial_production/index.php

Please transfer your token number to the space below.

Credit Card Token Number:

Cover Posters

Posters are available of all the published covers and frontispieces in two sizes

☐ DIN A2 42 x 60 cm / 17 x 24in (one copy: **39 Euro**)
☐ DIN A1 60 x 84 cm / 24 x 33in (one copy: **49 Euro**)

Postage for shipping posters overseas by airmail:
+ 25 Euro

Postage for shipping posters within Europe by surface mail:
+ 15 Euro

Price list for reprints (The prices include mailing and handling charges. All Wiley-VCH prices are exclusive of VAT)

No. of pages	Price (in Euro) for orders of					
	50 copies	100 copies	150 copies	200 copies	300 copies	500 copies
1-4	345	395	425	445	548	752
5-8	490	573	608	636	784	1077
9-12	640	739	786	824	1016	1396
13-16	780	900	958	1004	1237	1701
17-20	930	1070	1138	1196	1489	2022
for every additional 4 pages	147	169	175	188	231	315

★ **Special Offer** ★ If you order 200 or more reprints you will get a PDF file for half price.

Wiley-VCH Verlag GmbH & Co. KGaA; Location of the Company: Weinheim;
Chairman of the Supervisory Board: John Kritzmacher,
Trade Register: Mannheim, HRB 432833, General Partner: John Wiley & Sons GmbH,
Location: Weinheim, Trade Register Mannheim, HRB 432296,
Managing Directors: Sabine Steinbach, Dr. Guido F. Herrmann

WILEY-VCH